*13th International Conference on Applications of Statistics and Probability in Civil Engineering, ICASP13*
*Seoul, South Korea, May 26-30, 2019*

# Uncertainty Quantification of Tsunami Height for Future Earthquakes in West Japan

Takuya Miyashita
*Graduate Student, Dept. of Civil and Earth Resources Engineering, Kyoto Univ., Kyoto, Japan*

Nobuhito Mori
*Professor, Disaster Prevention Research Institute, Kyoto Univ., Kyoto, Japan*

Katsuichiro Goda
*Associate Professor, Dept. of Earth Sciences, Western Univ., London, Canada*

ABSTRACT: This study conducts probabilistic tsunami hazard analysis (PTHA) based on a random phase approximation developed by Goda et al. (2016). The target area and event are the western Japanese Pacific coast and the Nankai-Tonankai Earthquake. The result of a Monte Carlo tsunami simulation shows a large variations of tsunami height depending on the earthquake source and bathymetry. Following the tsunami simulation, probabilistic tsunami heights are estimated in two different approaches: the random phase and logic tree model. It is confirmed that exceedance probabilities of tsunami height differ significantly by the models.

## 1. INTRODUCTION

Future tsunami events are subjected to large uncertainties because of the complexity of earthquakes. In order to reflect these uncertainties, research on probabilistic tsunami hazard analysis/assessment (PTHA) has been developed and conducted worldwide. PTHA is analogous to probabilistic seismic hazard analysis (PSHA) which was developed in early 1960s (Cornell, 1968). Studies related to PTHA have been accelerated by two catastrophic events, the 2004 Indian Ocean tsunami and the 2011 Tohoku Japan tsunami (e.g. Mori et al., 2012). The most challenging problems are evaluating the modelling of the tsunami source and quantifying the variability of tsunami risks. These are essential to designing coastal structures and for planning facilities in coastal city areas.

PTHA studies have been conducted using several kinds of approaches (Mori et al., 2018). A major approach is the logic tree model (e.g., Geist and Parsons, 2006), which divides tsunami scenarios into a small number of branches and then estimates the probability of each branch using weights. Another is the random phase model, which is based on a Monte Carlo tsunami simulation and synthetic slip distributions with a random phase approximation (e.g., Goda et al., 2016). These approaches are different due to the assumptions of the earthquake source, and thus may lead to a crucial gap in the estimation of tsunami hazards and risks due to future events. However, both are regarded as valid PTHA approaches and their differences have been less documented. It is important to understand how large the differences of the probabilities are.

Along the Pacific coast of Japan, the Nankai-Tonankai region is particularly exposed to tsunami risk. Mega-thrust subduction earthquakes periodically occur in this region. To prepare for future events, the Central Disaster Management Council (CDMC), under the auspices of the Cabinet Office of the Japanese Government, has proposed 11 slip models with a moment magnitude of 9.0 as possi-

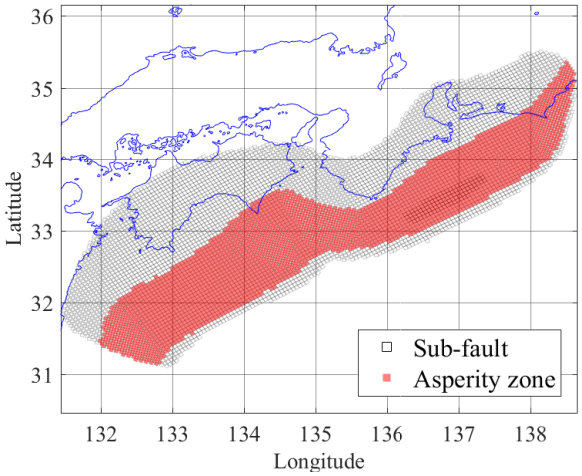


*Figure 1: Fault plane of the Nankai-Tonankai region assumed in this study. Its geometry and sub-faults are based on the CDMC 2012 model. There are 5699 sub-faults (5 km by 5 km in size each) in the plane. All of the squares represent sub-faults and red squares represent the asperity zone, which is determined by the top-fault depth.*

ble scenarios (hereafter, the 2012 CDMC model). However, the 11 models are intended to capture the range of tsunami hazard predictions. So their uncertainty quantification may be considered to be limited or less rigorous. More accurate tsunami assessment in this region is required to mitigate tsunami hazard and risk.

This paper is organized as follows. Section 2 presents a procedure for generating synthetic earthquake slips and stochastic tsunami simulations in the Nankai-Tonankai region. Section 3 provides the numerical simulation results and stochastic analysis. Tsunami heights along the shoreline are evaluated considering different earthquake rupture scenarios. It also provides a comparison of two different PTHA approaches, the random phase model and logic tree model. Finally, the main conclusions are discussed in Section 4.

## 2. METHODOLOGY

### *2.1. Synthetic rupture simulation*

In this section, methods of generating numerous earthquake rupture models and the numerical tsunami simulation are presented. The earthquake fault targeted in this study is a Nankai-Tonankai earthquake, located along the southwestern coast of Japan. First, the fault model needs to be defined. Figure 1 shows the fault model with 5699 sub-faults. The geometrical parameters of the sub-faults (e.g., top-fault depth, strike and dip) correspond to the 2012 CDMC model. This study defines a $M_w$9.0 earthquake as the worst scenario is this region, which is also based on the 2012 CDMC model. Additionally, other scenarios at different moment magnitudes are considered. There are in total 11 patterns of the moment magnitude, ranging from $M_w$ 8.0 to $M_w$ 9.0. The asperity region, shown in Figure 1 with the red boxes, is determined by the fault depth.

Earthquake source parameters are generated using scaling relationships as a function of $M_w$. The procedure of generating the source parameters and rupture models is briefly described in this paper; full details of the method can be found in Goda et al. (2016). First, the source parameters can be divided into three types: (i) geometry parameters including the fault width $W$ and fault length $L$; (ii) slip statistics parameters including mean slip $D_a$, maximum slip $D_m$, and Box-Cox power $\lambda$; and (iii) spatial slip distribution parameters including the correlation length along dip and strike directions $A_z$ and $A_x$ and the Hurst number $H$. Goda et al. (2016) developed a model that expresses key source earthquake parameters as a function of $M_w$ using statistical analyses of rupture models from the SRCMOD database (Mai and Thingbaijam, 2014). Regarding a tsunamigenic earthquake, source parameters except for $\lambda$ and $H$ had clear dependencies on $M_w$. Regression analysis was then carried out and the following functional form of the scaling relationship was obtained,

$$\log_{10}\theta(m,\varepsilon) = a_\theta + b_\theta m + \sigma_\theta \varepsilon, \qquad (1)$$

where $\theta$ is the source parameter of interest (e.g., $L$ and $W$), $m$ is the target moment magnitude, $\varepsilon$ is the standard normal variable and represents the randomness of the developed equation, $a_\theta$ and $b_\theta$ are the regression parameters, and $\sigma_\theta$ is the standard deviation of regression residuals, respectively. Using Eq. (1), normal random number $\varepsilon$, and $m$, the parameters correlated with the scale of $M_w$ can be

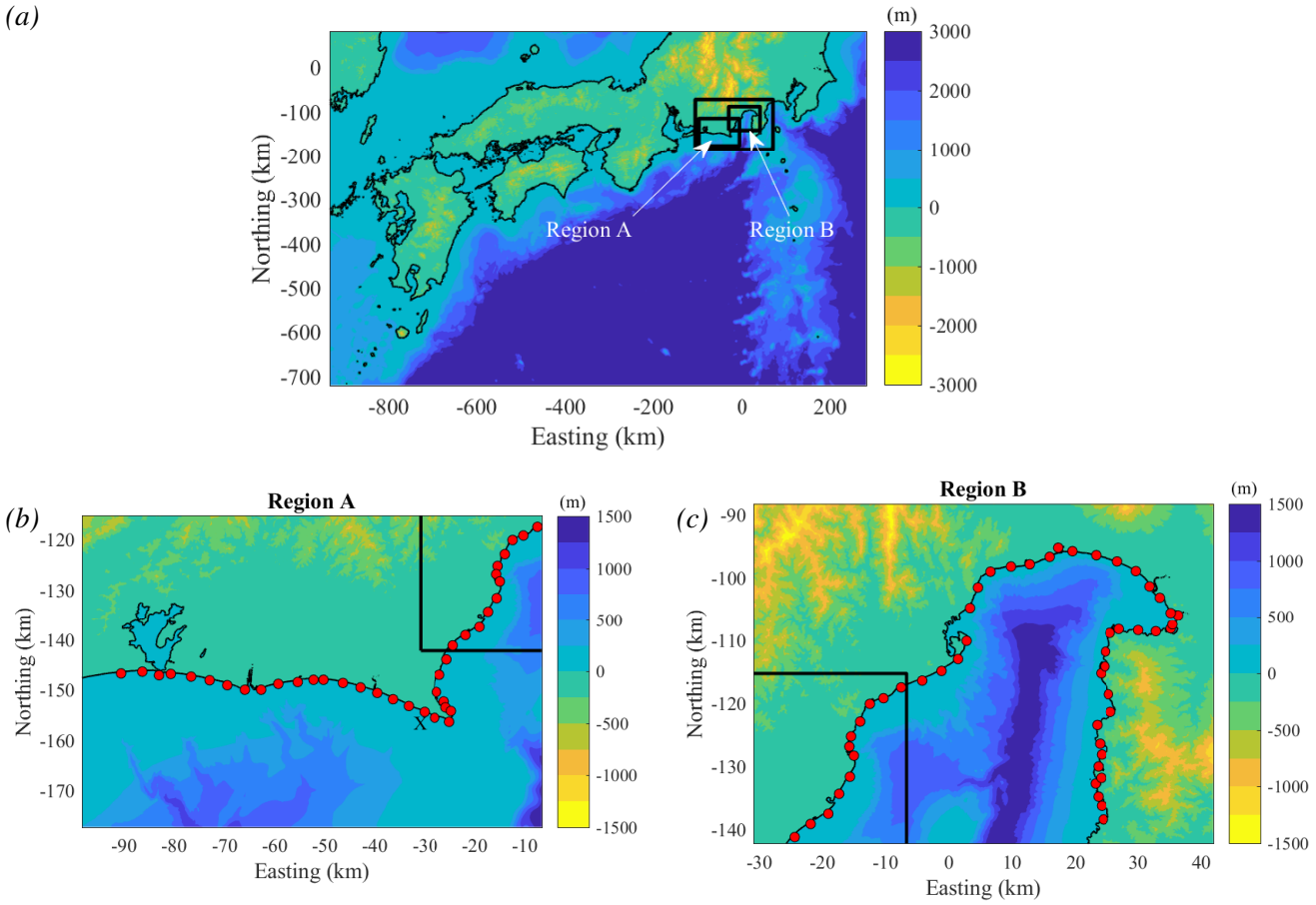


*Figure 2: Lower nested domains for the tsunami numerical simulations (2430 m grid is omitted). (a) The 810 m grid is shown with the nested 270 m and 90 m grids (indicated by the bold black squares). This study focuses on (b–c) the 90 m grid regions denoted Region A and Region B, respectively. Red circles in Regions A and B are the target points and a nuclear power plant is located behind the point labeled X. Thin black lines indicate coastlines.*

obtained. Here $\lambda$ and $H$ are independently generated with normal random numbers because no clear dependency on $M_w$ was observed.

Using the generated spatial distribution parameters, a random slip field is synthesized by a Fourier integral method. The amplitude spectrum of the target slip distribution is specified by the theoretical Fourier amplitude spectrum with $A_z$, $A_x$, and $H$ generated by the previous step. The phase spectrum is represented by a random phase matrix. Then, the synthesized slip is generated by combining the amplitude and phase spectrum. The synthesized slip distribution is converted via a Box-Cox transformation with $\lambda$. Subsequently, the position of the synthesized model is determined randomly within the source region. After that, the synthesized model is checked against several constraints. The constrains are based on the statistical analysis of inverted source models. If the synthesized model meets all of the constraints, it is accepted as a possible and realistic scenario in the target magnitude.

When these process are performed repeatedly, numerous rupture models are finally obtained. The procedure is repeated at 200 times for each $M_w$, thus in total 2200 rupture models are obtained. Then a Monte Carlo tsunami simulation is ready to be implemented.

### 2.2. *Monte Carlo tsunami simulation*

Tsunami numerical simulations are implemented using all synthetic rupture models. Figure 2 shows illustrations of the domains and bathymetry used

for the simulations. Bathymetry data are obtained from the Cabinet Office of the Japanese Government. There are five domains and four nested grids (2430, 810, 270, and 90 m), covering the geophysical regions of the Nankai-Tonankai Trough. The grid spacing of Figure 2 (a) is 810 m (second nest) and those of (b) and (c) are 90 m. Historically, the 1865 Ansei-Tokai earthquake tsunami struck around this region and the tsunami height was approximately 5 – 6 m from ground level according to the CDMC report.

The numerical model is based on the nonlinear shallow water equations, using a leap-frog staggered-grid finite-difference scheme. The governing and continuity equations are as follows:

$$\frac{\partial M}{\partial t}+\frac{\partial}{\partial x}\left(\frac{M^2}{D}\right)+\frac{\partial}{\partial y}\left(\frac{MN}{D}\right)= -gD\frac{\partial \eta}{\partial x}-\frac{\tau_x}{\rho}+A\left(\frac{\partial^2 M}{\partial x^2}+\frac{\partial^2 M}{\partial y^2}\right), \tag{2}$$

$$\frac{\partial N}{\partial t}+\frac{\partial}{\partial x}\left(\frac{MN}{D}\right)+\frac{\partial}{\partial y}\left(\frac{N^2}{D}\right)= -gD\frac{\partial \eta}{\partial y}-\frac{\tau_y}{\rho}+A\left(\frac{\partial^2 N}{\partial x^2}+\frac{\partial^2 N}{\partial y^2}\right), \tag{3}$$

and

$$\frac{\partial \eta}{\partial t}+\frac{\partial M}{\partial x}+\frac{\partial N}{\partial y}=0, \tag{4}$$

where $t$ is time, $x$ and $y$ are horizontal axes, $\eta$ is sea surface elevation, $M$ and $N$ are the discharge fluxes in the $x$ and $y$ directions, $g$ is the gravitational acceleration, $\rho$ is density of water, $D$ is the total depth, $\tau_x$ and $\tau_y$ are the bottom friction in the $x$ and $y$ directions, and $A$ the horizontal eddy viscosity. The initial water surface elevation is calculated by the Okada (1985) and Tanioka and Satake (1996) formulas. The simulation is performed for a 3 h duration, which is sufficient to model wave propagation in the Nankai-Tonankai region. The results of the Monte Carlo simulation are shown in the next section.

## 3. ANALYSIS

### *3.1. Variability of the maximum tsunami height*

Variability of the maximum tsunami heights due to the slip characteristics are examined. Figure 3 shows the means and standard deviations (SDs) of the maximum tsunami heights based on the 200 synthetic rupture models at $M_w$ 9.0. Regarding the mean of region A, an amplification of tsunami heights due to the bathymetry change is observed. This is consistent with the wave shoaling effect; the wave height is proportional to $h^{-1/4}$ where $h$ is depth ratio. In contrast with region A, the mean in region B does not correspond to the $h$ distribution. The western and eastern sides of the inner part of the bay show different tsunami heights; the differences are larger than 2 m. In addition, the SD is larger at the southwestern part of region B, which is behind the point of land on the eastern side of region A. This indicates that the wave shoaling is less dominant for tsunami heights inside the bay. Other physical processes , such as refraction, diffraction and direction of the tsunami source, have an influence on tsunami height.

Figure 4 shows the distributions of the simulated tsunami heights at the point X. The box plots are plotted for every 0.2 magnitude, which means that the amount of energy released by a larger earthquake is twice as a smaller one. It can be observed that the median of the tsunami heights is approximately equal to or slightly larger than the 0.75 fractile (the right edge of the box) for a 0.2 smaller magnitude. Large variability of tsunami heights can be seen for the same $M_w$. Furthermore, depending on the source characteristics and location, a tsunami event of $M_w$ 8.0 may result in a larger tsunami height than a $M_w$ 9.0 event, even though there is approximately 32 times difference of the total energy between the two possible events. It should be also noted that at least a 2.5 m tsunami occurs at $M_w$ 9.0 and this height is significantly larger than the smallest events of $M_w$ 8.8. Because the ruptured area for a $M_w$ 9.0 event is large enough to cover the entire fault, any resulting tsunami can affect this region significantly.

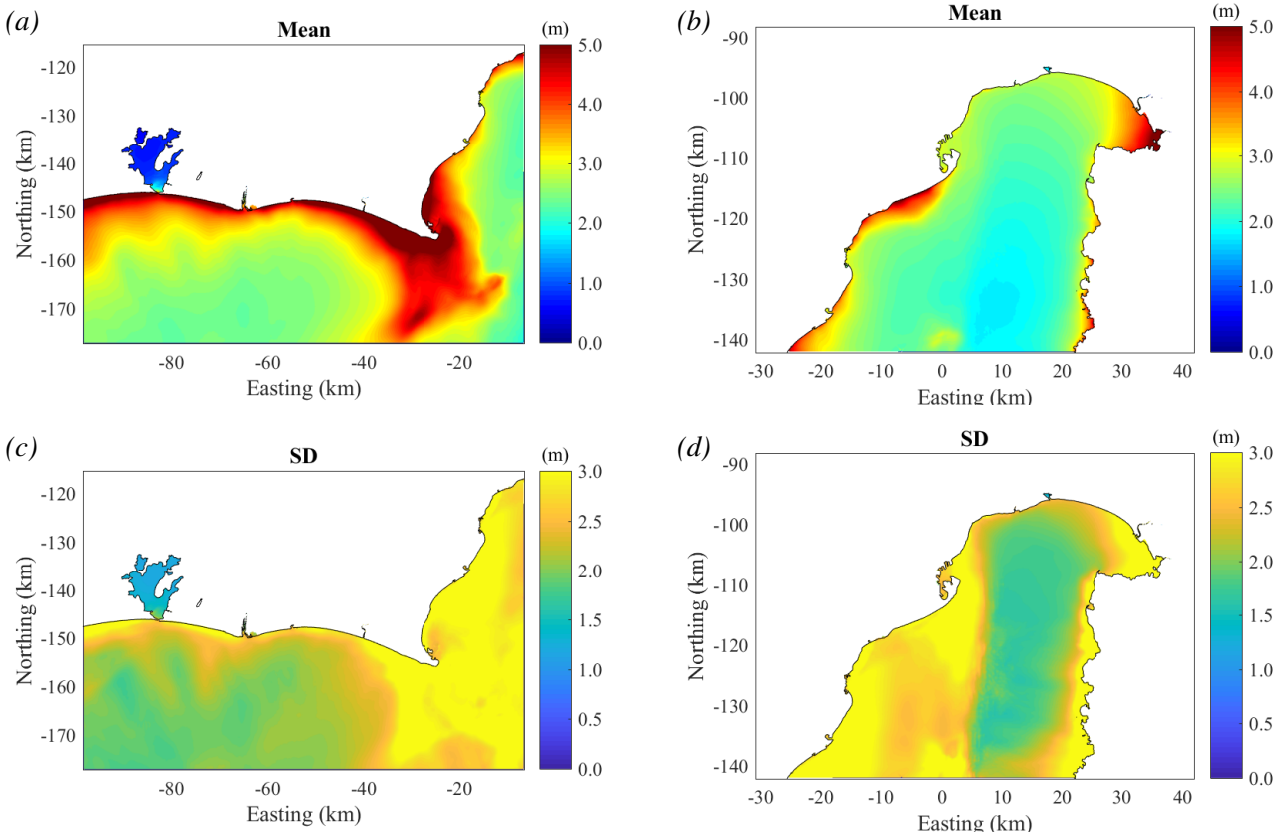


*Figure 3: Means and standard deviations (SDs) of the maximum tsunami heights for the* $M_W$ 9.0 *scenario from the stochastic tsunami simulation: (a) mean in Region A, (b) mean in Region B, (c) SD in Region A, and (d) SD in Region B.*

### *3.2. Comparison of PTHA approaches*

Exceedance probabilities of the tsunami heights are obtained by two different models and compared. In the random phase model, a cumulative distribution function (CDF) of the tsunami height is calculated using all of the tsunami simulation results for each $M_w$. Then, the exceedance probability $p(\mathbf{r},\eta,m)$ is derived from $1-\text{CDF}$, where $\mathbf{r}$ is the location vector. Taking the annual occurrence rate into account and integrating $m$, the annual exceedance probability $P(\mathbf{r},\eta)$ (hazard curve) is obtained as follows,

$$P(\mathbf{r},\eta) = \int_m n(m)\cdot p(\mathbf{r},\eta,m)\, dm, \qquad (5)$$

where n is the annual occurrence rate. In this study, $n$ is determined by the Gutenberg-Richter (GR) law,

$$\log_{10} n(m) = a - b\,m, \qquad (6)$$

where a and b are parameters that depend on the source region.

The probability curve in the logic tree model needs to be calculated. Figure 5 shows the logic tree constructed in this study. The logic tree is based on Annaka et al. (2007) and Fukutani et al. (2015), which estimated the hazard curves targeting the east coast of Japan. These studies considered 2–5 rupture models as the branch for the position of asperity. In order to compare the estimation of the random phase, this study extracts five models from 200 synthesized rupture models for each $M_w$. The process of choosing the rupture models for the logic tree is as follows. First, the rupture models are classified into five types of location depending on the positions of the asperities. Then, the error $E$ from the scaling relationship with $M_w$ is calculated by the following formula:

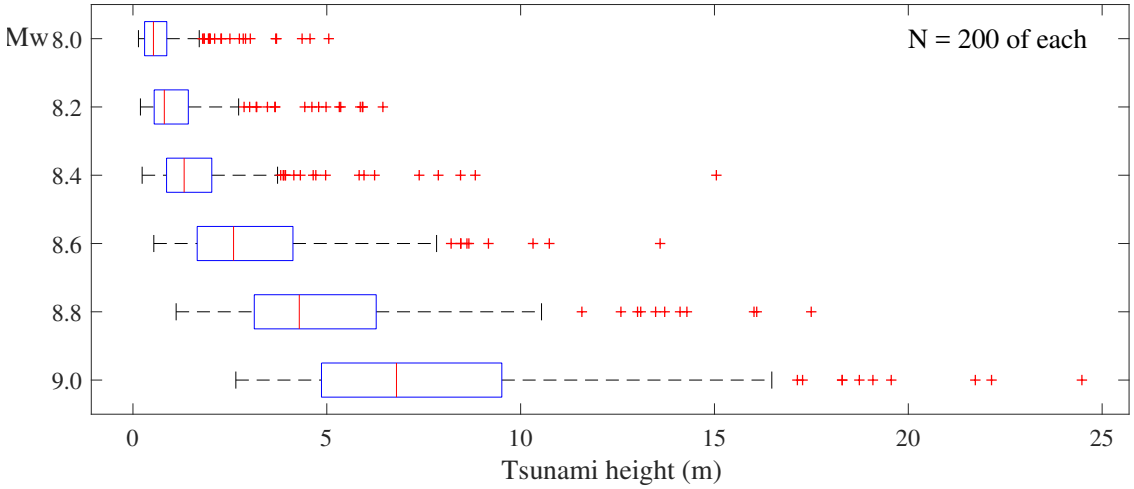


*Figure 4: Ranges of the simulated tsunami heights for 5 patterns of* $M_w$. *For each box, the central mark (red line) indicates the median, and the left and right edges of the blue box indicate the 0.25 and 0.75 fractiles; the whiskers (dashed lines) extend to the most extreme data points not considered outliers, and the red + symbols are the outliers.*

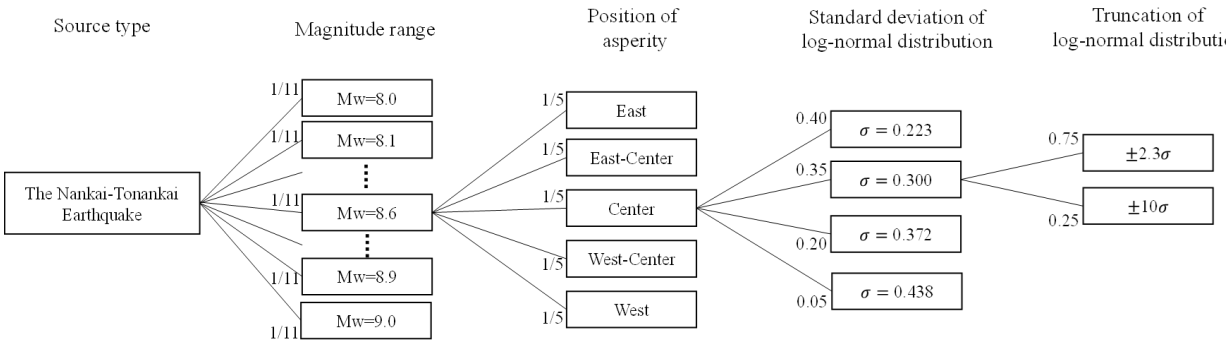


*Figure 5: Logic tree constructed in this study. There are four kinds of branches: magnitude, position of asperity, log normal standard deviation, and truncated range of the deviation. The numbers labeled at the branches indicate the weights. The weights and branches are based on previous logic tree studies in Japan. The recurrence interval of an earthquake is not considered because this study defines the occurrence rate using the G-R law.*

$$E(m) = \sum_i \frac{|\theta_i(m,\varepsilon) - \theta_i(m,0)|}{\theta_i(m,0)} \qquad (7)$$

After that, the rupture models which have a minimum $E$ among the same locations are extracted. In total, 55 rupture models (5 rupture models $\times$ 11 patterns of magnitude) are considered in the logic tree model. Figure 6 shows the five rupture models considered for the $M_w$ 8.0 case of the logic tree model.

It should be noted that the logic tree in this study excludes any kind of branch related to the recurrence interval of the earthquake in order to compare with tsunami heights and probabilities derived by the random phase model. In other words, the annual occurrence rate defined by the GR law is used for the logic tree model as well. Other branches and their weights are the same as the previous research. There are 440 ($11\times5\times4\times2$) paths in the logic tree. The annual exceedance probabilities are calculated based on the logic tree shown in Figure 5. In Figure 7, the hazard curves are shown for point X obtained by each path of the logic tree. A certain fractile of the curve is obtained by calculating the cumulative weights of height $\eta$.

Figure 8 shows a comparison of the hazard

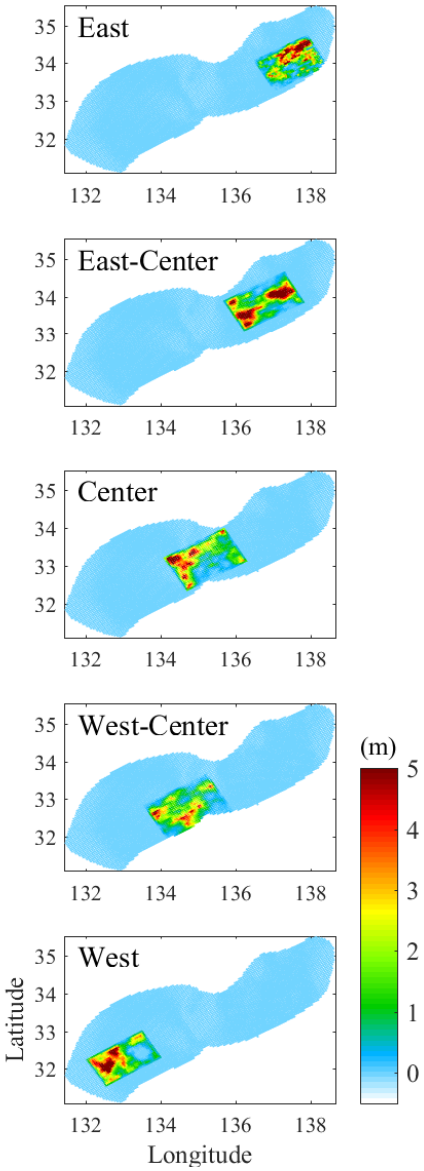


*Figure 6: Synthetic rupture models considered in the logic tree. The positions of asperity are uniformly distributed.*

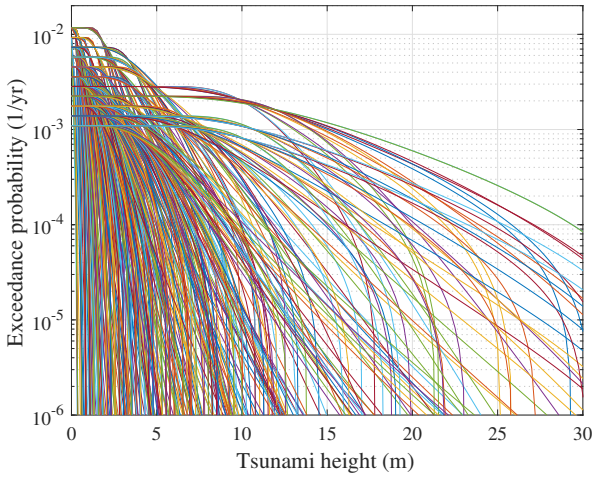


*Figure 7: All of the hazard curves obtained by each path of the logic tree. The number of the curves is 440.*

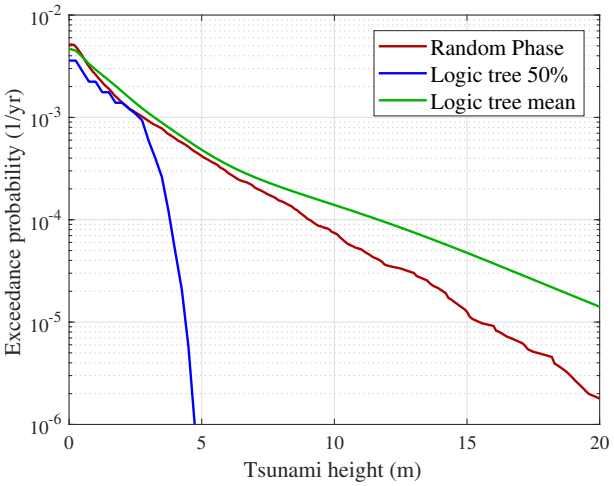


*Figure 8: Estimated probability curves in the two different models: random phase (red), logic tree 0.5 fractile (blue), and logic tree simple mean (green).*

curves obtained in the two different PTHA models. The logic tree for 50 %, often used for the single representation of a hazard, is the 0.5 fractile of the cumulative weight. The logic tree mean is the mean of the probability of each path. A radical decrease of the exceedance probability occurs in tsunami heights over 3 m. Consequently, a large difference between the random phase model and the logic tree model is observed. The annual exceedance probability in the logic tree 50 % is 100 times less than that in the random phase model when the tsunami is 5 m. This is caused by the number of rupture models taken into account and the truncation in the logic tree. In this study, some of the rupture models necessarily occur far from regions A and B. On the other hand, the mean hazard curve of the logic tree model are close to values of the random phase model. However, when analyzing Figures 7 and 8, most of the probabilities in the logic tree model are below its mean values. As such, the mean probability of the logic tree model highly depends on the extreme events.

## 4. CONCLUSIONS

In this study, a stochastic tsunami simulation based on synthetic earthquake rupture models is carried out for the future Nankai-Tonankai earthquake. A series of the synthetic rupture models takes into account the uncertainty of the intensity of earthquakes, key source parameters and locations. The result of the stochastic simulation indicates that an extreme event of $M_w$ 8.0 can cause a larger tsunami height than a $M_w$ 9.0 event. Additionally, mean values of the tsunami height differ depending on points within a bay, even in a case of the same moment magnitude.

Using the stochastic simulation, the relationships between annual exceedance probability and tsunami height are estimated in two different approaches: the logic tree and the random phase model. Compared with the random phase model and the mean logic tree model, the median logic tree model tends to estimate lower probabilities when the tsunami is high, and the difference can be over 100 times. The branches and their weights of the logic tree model cause the significant gap in the estimation of the probability. Therefore, the median logic tree model heavily depends on the epistemic uncertainty. The difference between the random phase model and the mean logic tree model is relatively small and the shapes of the hazard curves are similar since the random phase model is inherently the mean estimate. The difference in higher tsunami comes from the number of rupture models and how they are taken account in the logic tree model. Consequently, the process of choosing the rupture models are significant in the logic tree model.

## 5. REFERENCES

Annaka, T., Satake, K., Sakakiyama, T. Yanagisawa, K., and Shuto, N. (2007). "Logic-tree approach for probabilistic tsunami hazard analysis and its applications to the japanese coasts." *Tsunami and Its Hazards in the Indian and Pacific Oceans*, 58, 577–592.

Cornell, C. A. (1968). "Engineering seismic risk analysis." *Bulletin of the Seismological Society of America*, 58(5), 1583–1606.

Fukutani, Y., Suppasri, A., and Imamura, F. (2015). "Stochastic analysis and uncertainty assessment of tsunami wave height using a random source parameter model that targets a tohoku-type earthquake fault." *Stochastic Environmental Research and Risk Assessment*, 29(7), 1763–1779.

Geist, E. and Parsons, T. (2006). "Probabilistic analysis of tsunami hazards." *Stochastic Environmental Research and Risk Assessment*, 37(3), 277–314.

Goda, K., Yasuda, T., Mori, N., and Maruyama, T. (2016). "New scaling relationships of earthquake source parameters for stochastic tsunami simulation." *Coastal Engineering Journal*, 58(3), 1650010.

Mai, P. M. and Thingbaijam, K. K. S. (2014). "SRCMOD: An online database of finite fault rupture models." *Seismological Research Letters*, 85(6), 1348–1357.

Mori, N., Goda, K., and Cox, D. (2018). "Recent process in probabilistic tsunami hazard analysis (ptha) for mega thrust subduction earthquakes." *The 2011 Japan Earthquake and Tsunami: Reconstruction and Restoration. Advances in Natural and Technological Hazards Research*, 47, 469–485.

Mori, N., Takahashi, T., and The 2011 Tohoku Earthquake Tsunami Joint Survey Group (2012). "Nationwide post event survey and analysis of the 2011 tohoku earthquake tsunami." *Coastal Engineering Journal*, 54(1).

Okada, Y. (1985). "Surface deformation due to shear and tensile faults in a half-space." *Bulletin of the Seismological Society of America*, 75(4), 1135–1154.

Tanioka, Y. and Satake, K. (1996). "Tsunami generation by horizontal displacement of ocean bottom." *Geophysical Research Letters*, 23(8), 861–864.